Mass imbalance effect in resonant Bose-Fermi mixtures

Elisa Fratini and Pierbiagio Pieri
School of Science and Technology, Physics Division, University of Camerino and CNISM, Via Madonna delle Carceri 9, I-62032 Camerino, Italy
(Received 19 December 2011; published 26 June 2012)

We consider a homogeneous Bose-Fermi mixture, with the boson-fermion interaction tuned by a Fano-Feshbach resonance, in the presence of mass and density imbalance between the two species. By using many-body diagrammatic methods, we first study the finite-temperature phase diagram for the specific case of the mass-imbalanced mixture ^{87}Rb-^{40}K for different values of the density imbalance. We then analyze the quantum phase transition associated with the disappearance at zero temperature of the boson condensate above a critical boson-fermion coupling. We find a pronounced dependence of the critical coupling on the mass ratio and a weak dependence on the density imbalance. For a vanishingly small boson density, we derive, within our approximation, the asymptotic expressions for the critical coupling in the limits of small and large mass ratios. These expressions are relevant also for the polaron-molecule transition in a Fermi mixture at small and large mass ratios. The analysis of the momentum distribution functions at sufficiently large density imbalances shows an interesting effect in the bosonic momentum distribution due to the simultaneous presence of composite fermions and unpaired fermions.

DOI: 10.1103/PhysRevA.85.063618 PACS number(s): 03.75.Ss, 03.75.Hh, 32.30.Bv, 74.20.−z

I. INTRODUCTION

An impressive series of experiments has been realized with ultracold atomic gases over the last few years, reproducing systems, or physical situations, relevant to several areas of physics. The use of Fano-Feshbach resonances to control the interaction strength between particles, in particular, has been the cornerstone of many of these recent experimental achievements.

Besides providing analog quantum models and simulators for systems of interest in different fields of physics, ultracold gases offer also the possibility to construct novel many-body systems with no corresponding counterparts in other domains of physics. Resonant Bose-Fermi mixtures constitute an interesting example in this respect and have been the object of active theoretical and experimental investigation recently.

Nonresonant Bose-Fermi mixtures were initially studied theoretically and experimentally in Refs. [1–7] and [8], respectively. Bose-Fermi mixtures in the presence of a *narrow* Fano-Feshbach resonance were then considered in the theoretical works of Refs. [9–13]. For a narrow resonance one has to take into account explicitly the molecular state forming in the closed channel, leading to a Hamiltonian which includes three different species (bosons, fermions, and molecules) from the outset.

Both cases of narrow or broad resonance are, however, relevant to current experiments in Bose-Fermi mixtures [14–21], depending on the mixture and/or resonance actually chosen in the experiment. A broad Fano-Feshbach resonance is characterized by the smallness of the effective range parameter r_0 of the boson-fermion scattering amplitude with respect to both the average interparticle distance and the boson-fermion scattering length a [22]. Under these conditions, the system can be described by a Hamiltonian made just by bosons and fermions mutually interacting via an attractive contact potential.

Initial works studying Bose-Fermi mixtures in the presence of a broad resonance focused on lattice models [23–28] or considered separable interactions, as inspired by nuclear-physics models [29]. The continuum case in the presence of an attractive contact potential was first tackled in Ref. [30], which concentrated on the thermodynamic properties of the condensed phase of a Bose-Fermi mixture at zero temperature.

A study of the competition between Bose-Fermi pairing and boson condensation in a broadly resonant Bose-Fermi mixture has been presented in a previous work by us [31]. By using many-body diagrammatic theory, with a T-matrix approximation for the bosonic and fermionic self-energies, we were able to show that, for increasing Bose-Fermi attraction, the boson-fermion pairing correlations progressively reduce the boson condensation temperature and make it eventually vanish at a critical coupling above which the condensate is completely depleted (thus revealing the presence of a quantum phase transition at zero temperature). In the present paper we extend the work of Ref. [31] by analyzing the effect of a mass imbalance between the bosonic and fermionic species. We present results both at finite temperature (for a specific mass ratio) and at zero temperature (for several mass ratios). The effect of mass imbalance in a broadly resonant Bose-Fermi mixture has been studied recently also in Ref. [32], within a path-integral approach which is complementary to our approach and that was limited to zero temperature only. A comparison between our results and those of Ref. [32] will be discussed later on in our paper.

The paper is organized as follows: In Sec. II we present the theoretical formalism and the main equations describing the physical system of interest in our paper. Section III reports the numerical results at finite temperature for a ^{87}Rb-^{40}K mixture. The phase diagram for different values of density imbalance is presented, together with the curves for the boson and fermion chemical potentials at the critical temperature. Section IV treats the zero-temperature limit. We report the results for the dependence of critical coupling on mass ratio and density imbalance, the corresponding chemical potentials, and the momentum distribution functions. Section V presents finally our conclusions.

II. FORMALISM

We consider a homogeneous mixture composed of single-component fermions and bosons. The boson-fermion interaction is assumed to be tuned by a broad Fano-Feshbach resonance, as in most current experiments on Bose-Fermi mixtures [14–20]. Under this condition, the boson-fermion interaction can be adequately described by an attractive point-contact potential. We consider then the following (grand-canonical) Hamiltonian:

$$H = \sum_s \int d\mathbf{r}\psi_s^\dagger(\mathbf{r})\left(-\frac{\nabla^2}{2m_s} - \mu_s\right)\psi_s(\mathbf{r}) + v_0 \int d\mathbf{r}\psi_{\mathrm{B}}^\dagger(\mathbf{r})\psi_{\mathrm{F}}^\dagger(\mathbf{r})\psi_{\mathrm{F}}(\mathbf{r})\psi_{\mathrm{B}}(\mathbf{r}). \quad (1)$$

Here $\psi_s^\dagger(\mathbf{r})$ creates a particle of mass m_s and chemical potential μ_s at spatial position $\mathbf{r}$, where $s = \mathrm{B,F}$ indicates the boson and fermion atomic species, respectively, while v_0 is the bare strength of the contact interaction (we set $\hbar = k_{\mathrm{B}} = 1$ throughout this paper). As for two-component Fermi gases [33], the ultraviolet divergences associated with the contact interaction in Eq. (1) are eliminated by expressing the bare interaction v_0 in terms of the boson-fermion scattering length a:

$$\frac{1}{v_0} = \frac{m_r}{2\pi a} - \int \frac{d\mathbf{k}}{(2\pi)^3}\frac{2m_r}{\mathbf{k}^2}, \quad (2)$$

where $m_r = m_{\mathrm{B}}m_{\mathrm{F}}/(m_{\mathrm{B}} + m_{\mathrm{F}})$ is the reduced mass of the boson-fermion system.

We have not considered in the Hamiltonian (1) an explicit boson-boson interaction term. In the physical systems relevant to experiments, the corresponding nonresonant scattering length is normally small and positive. In the homogeneous and normal system we are going to consider, it yields then only a mean-field shift of the boson chemical potential. Note, however, that according to the variational analysis of Ref. [34], the assumption of having a homogeneous system actually requires the boson-boson scattering length to exceed a certain value, in order to guarantee the mechanical stability of the Bose-Fermi mixture against collapse. We thus implicitly assume to work in this stable regime. Note finally that a Fermi-Fermi s-wave scattering length is excluded by Pauli principle.

A natural length scale for the system is provided by the average interparticle distance $n^{-1/3}$ (where $n = n_{\mathrm{B}} + n_{\mathrm{F}}$ is the total particle-number density, n_{B} and n_{F} being the individual boson and fermion particle-number density, respectively). We thus introduce a fictitious Fermi momentum of the system $k_{\mathrm{F}} \equiv (3\pi^2 n)^{1/3}$ (as for an equivalent two-component Fermi gas with a density equal to the total density of the system) and use the dimensionless coupling parameter $g = (k_{\mathrm{F}}a)^{-1}$ to describe the strength of the interaction. In the weak-coupling limit, where the scattering length a is small and negative and $g \ll -1$, the two components behave essentially as Bose and Fermi ideal gases. In the opposite, strong-coupling limit where a is small and positive and $g \gg 1$, the system is expected to be be described in terms of composite fermions [i.e., boson-fermion pairs with a binding energy $\epsilon_0 = 1/(2m_r a^2)$] and excess fermions. (We restrict our analysis to mixtures where the number of bosons never exceeds the number of fermions because only in this case is a quantum phase transition associated with the disappearance of the condensate possible [31]. In addition, mixtures with $n_{\mathrm{B}} > n_{\mathrm{F}}$ are expected to be severely affected by three-atom losses). The physical behavior of a Bose-Fermi mixture across all the resonance is captured by the T-matrix set of diagrams for the boson and fermion self-energies represented in Fig. 1. As shown in our previous work [31], this set of diagrams is able to recover the expected physical behavior in both the weak- and strong-coupling limits, thus providing a meaningful theoretical framework for the whole resonance. The corresponding equations for the bosonic and fermionic self-energies Σ_{B} and Σ_{F} and many-body T matrix Γ read

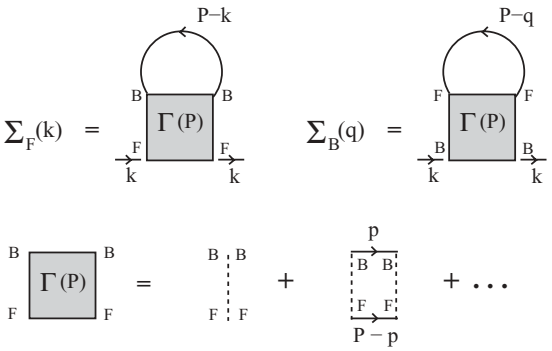

FIG. 1. (Color online) T-matrix diagrams for the fermionic and bosonic self-energies in the normal phase. Full lines represent bare bosonic (BB) and fermionic (FF) Green's functions. Broken lines represent bare boson-fermion interactions v_0.

$$\Sigma_{\mathrm{B}}(q) = -T\int \frac{d\mathbf{P}}{(2\pi)^3}\sum_m G_{\mathrm{F}}^0(P-q)\Gamma(P), \quad (3)$$

$$\Sigma_{\mathrm{F}}(k) = T\int \frac{d\mathbf{P}}{(2\pi)^3}\sum_m G_{\mathrm{B}}^0(P-k)\Gamma(P), \quad (4)$$

$$\Gamma(\mathbf{P},\Omega_m) = -\left\{\frac{m_r}{2\pi a} + \int\frac{d\mathbf{p}}{(2\pi)^3} \times\left[\frac{1 - f\left[\xi_{\mathrm{F}}(\mathbf{P}-\mathbf{p})\right] + b\left[\xi_{\mathrm{B}}(\mathbf{p})\right]}{\xi_{\mathrm{F}}(\mathbf{P}-\mathbf{p}) + \xi_{\mathrm{B}}(\mathbf{p}) - i\Omega_m} - \frac{2m_r}{\mathbf{p}^2}\right]\right\}^{-1}. \quad (5)$$

Here $q = (\mathbf{q},\omega_\nu)$, $k = (\mathbf{k},\omega_n)$, $P = (\mathbf{P},\Omega_m)$, where $\omega_\nu = 2\pi\nu T$ and $\omega_n = (2n+1)\pi T$, $\Omega_m = (2m+1)\pi T$ are bosonic and fermionic Matsubara frequencies, respectively, (ν,n,m being integer numbers), while $f(x)$ and $b(x)$ are the Fermi and Bose distribution functions at temperature T, and $\xi_s(\mathbf{p}) = \mathbf{p}^2/(2m_s) - \mu_s$.

The self-energies (3) and (4) determine the dressed Green's functions G_s via the Dyson's equation $G_s^{-1} = G_s^{0\,-1} - \Sigma_s$ (with the bare Green's functions given by $G_{\mathrm{B}}^0(q) = [i\omega_\nu - \xi_{\mathrm{B}}(\mathbf{q})]^{-1}$ and $G_{\mathrm{F}}^0(k) = [i\omega_n - \xi_{\mathrm{F}}(\mathbf{k})]^{-1}$). The dressed Green's functions G_s allow us to calculate the boson and fermion momentum distribution functions through the equations

$$n_{\mathrm{B}}(\mathbf{q}) = -T\sum_\nu G_{\mathrm{B}}(\mathbf{q},\omega_\nu)e^{i\omega_\nu 0^+}, \quad (6)$$

$$n_{\mathrm{F}}(\mathbf{k}) = T\sum_n G_{\mathrm{F}}(\mathbf{k},\omega_n)e^{i\omega_n 0^+}, \quad (7)$$

which in turn determine the boson and fermion number densities

$$n_{\mathrm{B}} = \int \frac{d\mathbf{q}}{(2\pi)^3} n_{\mathrm{B}}(\mathbf{q}), \tag{8}$$

$$n_{\mathrm{F}} = \int \frac{d\mathbf{k}}{(2\pi)^3} n_{\mathrm{F}}(\mathbf{k}). \tag{9}$$

At fixed densities and temperature, the two coupled equations (8) and (9) fully determine the boson and fermion chemical potentials and, therefore, the thermodynamic properties of the Bose-Fermi mixture in the normal phase.

Coming from the normal phase, the condensation of bosons starts when the condition

$$\mu_{\mathrm{B}} - \Sigma_{\mathrm{B}}(q = 0) = 0, \tag{10}$$

is first met. Equation (10) corresponds to the requirement of a divergent occupancy of the boson momentum distribution at zero momentum: $\lim_{\mathbf{q}\to\mathbf{0}} n_{\mathrm{B}}(\mathbf{q}) = \infty$ [35].

A. Zero-temperature limit

We pass now to consider the zero-temperature limit of the previous finite-temperature formalism. When $T \to 0$, the spacing $2\pi T$ between two consecutive Matsubara frequencies tends to zero. The sums over discrete Matsubara frequencies can then be replaced by integrals over continuous frequencies, provided the corresponding integrands are not too singular [36]. We have then the equations

$$\Sigma_{\mathrm{B}}(q) = -\int \frac{d\mathbf{P}}{(2\pi)^3} \int \frac{d\Omega}{2\pi} G^0_{\mathrm{F}}(P - q)\Gamma(P), \tag{11}$$

$$\Sigma_{\mathrm{F}}(k) = \int \frac{d\mathbf{P}}{(2\pi)^3} \int \frac{d\Omega}{2\pi} G^0_{\mathrm{B}}(P - k)\Gamma(P), \tag{12}$$

for the bosonic and fermionic self-energies, where $q = (\mathbf{q},\omega_{\mathrm{B}})$, $k = (\mathbf{k},\omega_{\mathrm{F}})$, $P = (\mathbf{P},\Omega)$ while the frequencies ω_{B}, ω_{F}, and Ω are now continuous variables.

Similarly, the Eqs. (6) and (7) for the momentum distribution functions are changed to

$$n_{\mathrm{B}}(\mathbf{q}) = -\int \frac{d\omega_{\mathrm{B}}}{2\pi} G_{\mathrm{B}}(\mathbf{q},\omega_{\mathrm{B}}) e^{i\omega_{\mathrm{B}}0^+}, \tag{13}$$

$$n_{\mathrm{F}}(\mathbf{k}) = \int \frac{d\omega_{\mathrm{F}}}{2\pi} G_{\mathrm{F}}(\mathbf{k},\omega_{\mathrm{F}}) e^{i\omega_{\mathrm{F}}0^+}, \tag{14}$$

from which the number densities can be calculated as before.

A closed-form expression can be finally derived for the many-body T-matrix $\Gamma(P)$ at zero temperature, when the Fermi and Bose distribution functions appearing in Eq. (5) are replaced by step functions. We report in particular the expression for $\Gamma(P)$ when $\mu_{\mathrm{F}} > 0$ and $\mu_{\mathrm{B}} < 0$, which is in practice the only one relevant to our calculations at zero temperature.

We have

$$\Gamma(P) = -\left[\frac{m_r}{2\pi a} - \frac{m_r^{\frac{3}{2}}}{\sqrt{2}\pi}\sqrt{\frac{\mathbf{P}^2}{2M} - 2\mu - i\Omega} - I_{\mathrm{F}}(P)\right]^{-1}, \tag{15}$$

where we have defined $M = m_{\mathrm{B}} + m_{\mathrm{F}}$ and $\mu = (\mu_{\mathrm{B}} + \mu_{\mathrm{F}})/2$, while $I_{\mathrm{F}}(P)$, which results from the integration of the term with the Fermi function in Eq. (5), is given by

$$I_{\mathrm{F}}(P) = \frac{m_{\mathrm{B}}\left(k^2_{\mu_{\mathrm{F}}} - k^2_{\mathbf{P}} - k^2_{\Omega}\right)}{8\pi^2|\mathbf{P}|} \ln\left[\frac{(k_{\mu_{\mathrm{F}}} + k_{\mathbf{P}})^2 - k^2_{\Omega}}{(k_{\mu_{\mathrm{F}}} - k_{\mathbf{P}})^2 - k^2_{\Omega}}\right] - \frac{m_r k_{\Omega}}{4\pi^2}\left\{\ln\left[\frac{(k_{\mu_{\mathrm{F}}} + k_{\Omega})^2 - k^2_{\mathbf{P}}}{k^2_{\mathbf{P}} - (k_{\mu_{\mathrm{F}}} - k_{\Omega})^2}\right] - i\pi\,\mathrm{sgn}\,(\Omega)\right\} + \frac{m_r k_{\mu_{\mathrm{F}}}}{2\pi^2}, \tag{16}$$

where $k_{\mu_{\mathrm{F}}} \equiv \sqrt{2m_{\mathrm{F}}\mu_{\mathrm{F}}}$, $k_{\mathbf{P}} \equiv \frac{m_{\mathrm{F}}}{M} P$, while

$$k_{\Omega} \equiv (2m_r)^{\frac{1}{2}} \sqrt{-\frac{\mathbf{P}^2}{2M} + 2\mu + i\Omega}. \tag{17}$$

Equations (11)–(16) determine the thermodynamic properties of a Bose-Fermi mixture at zero temperature in the absence of boson condensation. They are thus relevant for a sufficiently strong coupling g, such that the system remains in the normal phase even at zero temperature. In particular, upon lowering the coupling constant g, the condensation will start at a critical coupling g_c, when the condition (10) is first satisfied.

III. FINITE-TEMPERATURE RESULTS

The theoretical approach developed in Sec. II can be used to explore the normal phase of a homogeneous Bose-Fermi mixture at arbitrary values of the boson and fermion masses and densities. In this section, where we present finite-temperature results, we focus on the specific mass ratio $m_{\mathrm{B}}/m_{\mathrm{F}} = 87/40$, relevant for the ^{87}Rb-^{40}K mixture. More general mass ratios will be considered at zero temperature.

A. Critical temperature

Figure 2 presents the dependence of the condensation critical temperature on the boson-fermion coupling $(k_{\mathrm{F}}a)^{-1}$ for a ^{87}Rb-^{40}K mixture, at different values of the density imbalance $(n_{\mathrm{F}} - n_{\mathrm{B}})/(n_{\mathrm{F}} + n_{\mathrm{B}})$. The critical temperature was obtained by numerically solving Eqs. (3)–(9), supplemented by the condition (10), while the ending point at $T = 0$ was

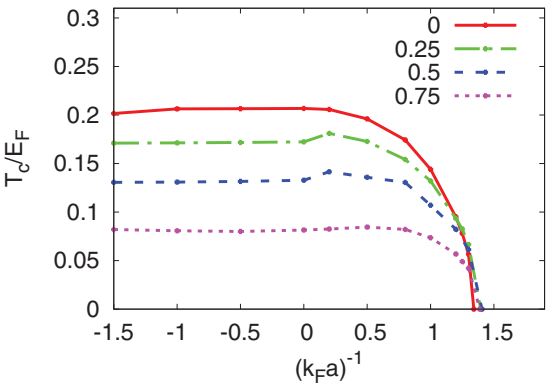

FIG. 2. (Color online) Critical temperature (in units of $E_{\mathrm{F}} = k^2_{\mathrm{F}}/2m_{\mathrm{F}}$) for condensation of bosons as a function of the boson-fermion coupling $(k_{\mathrm{F}}a)^{-1}$ for different values of the density imbalance $(n_{\mathrm{F}} - n_{\mathrm{B}})/(n_{\mathrm{F}} + n_{\mathrm{B}})$ in a mixture with $m_{\mathrm{B}}/m_{\mathrm{F}} = 87/40$.

calculated independently by solving the equations (11)–(16) [with the condition (10) defining now the critical coupling g_c at zero temperature]. The matching between finite-temperature and zero-temperature results confirms the validity of the equations derived in the zero-temperature limit, while providing simultaneously a check of the numerical calculations.

The overall behavior of the critical temperature as a function of coupling is similar to what is found for equal masses [31]. The critical temperature starts from the noninteracting value ($T_0 = 3.31 n_B^{2/3}/m_B$) in the weak-coupling limit and eventually vanishes at a critical coupling g_c, when the effect of the boson-fermion coupling is so strong that the Bose-Einstein condensate is completely depleted in favor of the formation of molecules. The weak dependence of the critical coupling on the density imbalance previously found for equal masses is confirmed also for this case with different masses. In this case, the critical coupling varies in the range 1.3–1.4, to be compared with the range 1.6–1.8 found for $m_B = m_F$.

A minor difference with respect to the case with equal masses is finally the presence of a weak maximum in the critical temperature, which reaches a value slightly above the noninteracting value T_0 before its final decrease. This feature is more pronounced for intermediate values of the density imbalance. We attribute this feature to the delicate balance between the effects of the boson-fermion interaction on the boson dispersion and to the condensate depletion due to molecular correlations. The boson dispersion may in fact be hardened by the interaction (similarly to what one finds for a dilute repulsive Bose gas [37]), thus leading to an increase in the critical temperature. The predominance of one effect over the other depends on a fine tuning of the mass ratio and density imbalance and may explain the different behavior found for different values of these parameters.

B. Chemical potentials

Figure 3 reports the coupling dependence of the chemical potentials μ_B and μ_F at the critical temperature for a ^{87}Rb-^{40}K mixture at the same values of density imbalance considered in Fig. 2.

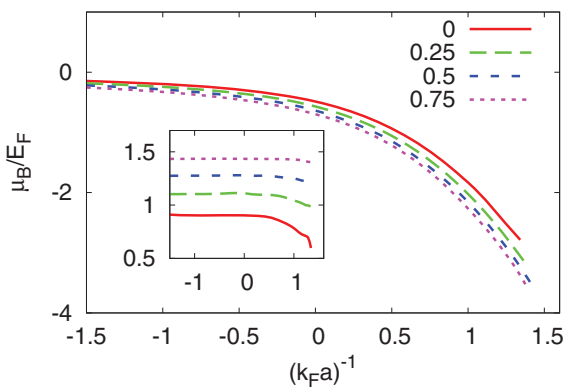

FIG. 3. (Color online) bosonic chemical potential at the critical temperature T_c as a function of the boson-fermion coupling $(k_F a)^{-1}$ for different values of the density imbalance $(n_F - n_B)/(n_F + n_B)$ in a mixture with $m_B/m_F = 87/40$. The corresponding fermionic chemical potential is reported in the inset.

In this case, the critical boson and fermion chemical potentials present the same qualitative behavior already found for a mixture with equal masses [31]. The boson chemical potential decreases markedly with increasing coupling, and changes from $\mu_B \approx 2\pi n_F a/m_r$ for weak coupling to $\mu_B \approx -\epsilon_0$ for strong coupling, with a small dependence on the density imbalance.

The fermion chemical potential (reported in the inset) remains, instead, almost constant across the whole resonance. The decrease of the chemical potential due to the attractive interaction with the bosons is, in fact, partially compensated by the decreasing of the temperature when moving along the critical line (which increases μ_F) and by the Pauli repulsion between unpaired fermions and Bose-Fermi pairs.

IV. ZERO-TEMPERATURE RESULTS

The behavior of the critical temperature as a function of the boson-fermion coupling discussed in the previous section is evidence of the presence of a quantum phase transition at zero temperature associated with a transition between a superfluid phase with a boson condensate to a normal phase, where the condensate is completely depleted. In this section we examine in more detail this quantum phase transition by solving numerically the equations formulated at exactly zero temperature.

A. Critical couplings and chemical potentials

Figure 4 reports the critical coupling g_c as a function of the mass ratio m_B/m_F, with two distinct panels for the cases $m_B/m_F \leqslant 1$ and $m_B/m_F \geqslant 1$. The different curves reported in Fig. 4 correspond to different values of the density imbalance, ranging from the density-balanced case to the fully imbalanced case $(n_F - n_B)/(n_F + n_B) = 1.0$, which represents the system with just one boson immersed in a Fermi sea. This is actually the same as a spin-down fermion surrounded by a Fermi sea of spin-up fermions, since for a single particle the statistics is irrelevant. The critical coupling reduces thus to that for the polaron-to-molecule transition, which was recently studied in the context of strongly imbalanced two-component Fermi gases [38–44]. The equations governing the one-boson limit are reported in the Appendix.

The critical coupling is strongly influenced by the mass ratio, especially for $m_B/m_F < 1$. In this case, for all values of the density imbalance, g_c increases very rapidly as m_B/m_F is decreased. For the single-boson problem, an asymptotic expansion of the equations determining g_c for $m_B/m_F \to 0$ yields

$$g_c \approx \frac{4 \times 2^{1/3}}{3\pi}\frac{m_F}{m_B} + \frac{32 \times 2^{1/3}}{15\pi} \tag{18}$$

$$\approx 0.535\frac{m_F}{m_B} + 0.856, \tag{19}$$

which proves quite accurate even before the asymptotic regime is reached (the deviation from the numerical solution is 15% for $m_B/m_F = 1$ and 2% for $m_B/m_F = 0.1$). [See the Appendix for the details of the derivation of Eq. (18).]

The rapid increase of the critical coupling for the polaron-to-molecule transition when $m_\downarrow \to 0$ was already noticed

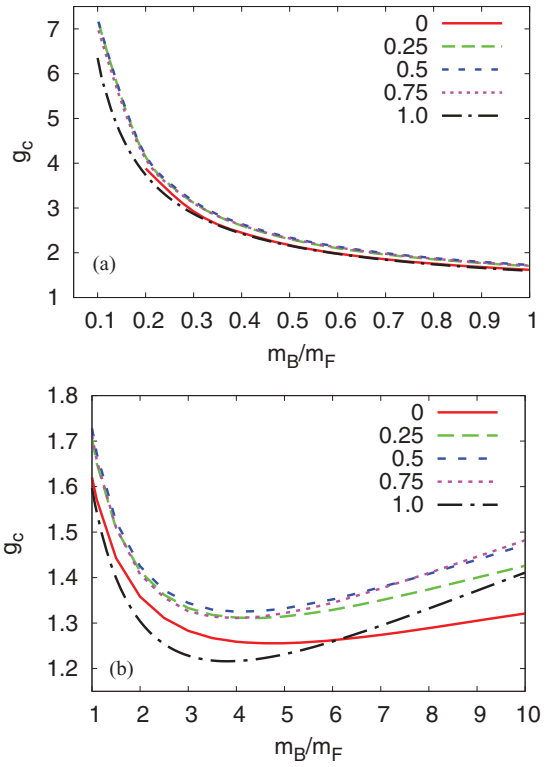

FIG. 4. (Color online) Critical coupling g_c as a function of the mass ratio (m_B/m_F) for different values of density imbalance $(n_F - n_B)/(n_F + n_B)$. Panels (a) and (b) correspond to the ranges $m_B/m_F \leqslant 1$ and $m_B/m_F \geqslant 1$, respectively.

in Ref. [43], even though no asymptotic expression was reported there. Note however that, according to the analysis of the polaron-to-molecule transition of Ref. [45], for a mass ratio $m_\downarrow/m_\uparrow \lesssim 0.15$ the molecular state acquires a finite momentum in its ground state. Similar results were obtained in Ref. [46]. The equations for the single-boson problem adopted here assume that the formation of the molecule occurs at zero center-of-mass momentum (as in Refs. [38–44]). The curve corresponding to the single-boson problem in Fig. 4 may thus change for $m_B/m_F \lesssim 0.15$, after taking into account the possibility of pairing at finite momentum. However, we expect this change to be minor on the basis of our calculations with a finite boson density, which allow for pairing at finite momentum and yield results close to the single-boson curve also for $m_B/m_F < 0.15$.

Note further that the study of the three-body system with two equal fermions with mass m_F and one different particle with mass m_B interacting through a zero-range potential, shows that, for $m_B/m_F < 0.0735 = (13.607)^{-1}$, the system is unstable due to a sequence of three-body bound states with energy $\to -\infty$ [47]. A similar instability is expected to occur also in the many-body system with N equal fermions plus one different particle (a recent work has proven indeed that the above critical value for the three-body system provides a lower bound for the location of the instability in the many-body system [48]). We note, however, that the unboundness from below of the Efimov spectrum (and the associated global instability) occurs only for a pure zero-range interaction. In a real system, physical two-body interactions will provide a natural cutoff at distances of the order of the van-der-Waals length r_{vdW}, thus limiting the position of the lowest Efimov level at an energy $\sim -1/r_{vdW}^2$. The global mechanical instability is thus avoided by the real system, even though the presence of Efimov states is expected to lead to an enhancement of three-body losses when they lie close to the three-particle or atom-dimer continuum. We further note in this context that the presence of the (nonuniversal) three-body bound states recently found by Kartavtsev and Malykh [49] for $(8.2)^{-1} > m_B/m_F > (13.607)^{-1}$ could also lead to enhanced three-body losses in this mass-ratio range.

We observe in any case that, since our calculations were taken for $m_B/m_F \geqslant 0.1$ ($m_B/m_F \geqslant 0.2$ for equal densities, due to numerical difficulties), the above three-body effects (which are beyond the scope of the present theory) should affect our study only marginally.

Consistently with our previous results, we observe a weak dependence of g_c on the density imbalance. Such a weak dependence on the densities remains valid also for $m_B > m_F$. In this case, all curves reach a minimum value of g_c (=1.2−1.3) for mass ratios m_B/m_F in the range 3.5–5, after which they increase slowly with mass ratio. For the single-boson problem with a large mass we have obtained the asymptotic expression (see Appendix):

$$g_c \approx A(m_B/m_F) - \frac{2^{2/3}}{A(m_B/m_F)} + \frac{16}{3\pi}\frac{1}{A(m_B/m_F)^2}, \quad (20)$$

where

$$A(m_B/m_F) = \frac{2^{4/3}}{\pi}\left(\ln\frac{4m_B}{m_F} - 2\right). \quad (21)$$

One can see from Eqs. (20) and (21) that, at large mass ratios, g_c increases very slowly, with a logarithmic dependence on the mass ratios. Due to this ln dependence the leading behavior, $g_c \approx (2^{4/3}/\pi)\ln(4m_B/m_F)$, is reached only at extremely large mass ratios. Equation (20), which includes the first two corrections to the leading behavior, provides a better approximation, the deviation from the numerical solution being 15% for $m_B/m_F = 20$ and 1.5% for $m_B/m_F = 100$.

The increasing behavior of g_c at both small and large mass ratios implies the existence of a minimum in the curve for g_c at intermediate mass ratios, consistent with the results of Fig. 4. Note, however, that in earlier work for the polaron-molecule transition, the critical coupling for the transition was found to move away from the Bose-Einstein–condensate (BEC) limit for increasingly heavier impurities. In particular, Ref. [43] reported that the critical coupling should approach the unitary limit for an infinitely heavy impurity. Similar results were also found in two dimensions by M. Parish [50] (with the critical coupling approaching the weak-coupling limit in this case). A reason for such a difference may be that our theory in the limit of a single boson reduces to the "first-level approximation" of Ref. [43], with no particle-hole dressing of the molecule (while the polaron is described with the same accuracy obtained with the variational wave function introduced by Chevy [51], which is deemed quite accurate for the polaron energy [43]). The

"second-level approximation" of Ref. [43] includes instead a particle-hole dressing of the molecule. This inclusion is sufficient to recover in the strong-coupling limit the correct dimer-fermion scattering length and shifts the position of the critical coupling for equal masses from the value $(k_F a)^{-1} = 1.27c$ (=1.60) to the value $0.88c$ (=1.11) (the factor $c = 2^{1/3}$ appears here because of a different definition of k_F between us and the above references). The eventual (slow) increase of g_c at large mass ratios could then be an artifact of the "first-order approximation." Calculations at large mass ratios with alternative methods (such as fixed-node or diagrammatic quantum Monte Carlo methods) could definitively clarify this issue.

At equal densities, our results for g_c as a function of mass ratio agree well with the results reported in Ref. [32] for the same case. This is because the equations used in Ref. [32] for calculating g_c correspond, in a diagrammatic formalism, to the same choice of the self-energy as ours, but with Dyson's equation expanded: $G = G_0 + G_0 \Sigma G_0$ instead of $G^{-1} = G_0^{-1} - \Sigma$. Even though such an expansion is justified only when Σ is small, apparently it leads only to minor differences in the values for g_c. For instance, for equal masses and densities we obtained $g_c = 1.62$, to be compared with $g_c = 1.66$ in Ref. [32].

According to the analysis of Ref. [32], however, only for sufficiently large values of the boson-boson scattering length a_B, the critical coupling g_c lies in a stable region of the phase diagram. For small values of a_B, the second-order quantum phase transition between a condensed phase and a normal phase is in fact superseded by a phase separation between the two phases. According to our calculations, the compressibility matrix $\partial n_s / \partial \mu_{s'}$ is always positive in the normal phase, indicating that the second-order phase transition here explored lies, at worst, in a metastable region of the phase diagram. In order to examine its absolute stability within our approach, one should extend our study to the superfluid phase and make a comparison of the free energies for the normal and superfluid phases. This nontrivial extension is postponed to future work. We observe however, that if ratios a_B/a of the order of 0.2–0.3 are sufficient to suppress phase separation in most of the phase diagram (as the results of Ref. [32] seem to indicate), then the effect of a_B on g_c will be minor.

The weak dependence of the critical coupling on the density imbalance is emphasized in Fig. 5, which presents g_c as a function of density imbalance for some representative values of the mass ratio m_B/m_F. All curves show a weak dependence on the density imbalance, with a weak maximum at an intermediate imbalance (=0.55 for equal masses, and similarly for the other mass ratios considered here).

Figure 6 reports the chemical potentials at g_c as a function of mass ratio m_B/m_F for different density imbalances. As can be seen from the main panel, the (negative) bosonic chemical potential increases very rapidly in absolute value for $m_B/m_F \to 0$. This is because at g_c the bosonic chemical potential is already close to its strong-coupling limit, $\mu_B \approx -\epsilon_0$, such that the dimensionless ratio $|\mu_B|/E_F \approx 2g^2 m_F/m_r$. Since $g_c \sim m_F/m_B$ for $m_B \to 0$, we have $|\mu_B|/E_F \sim (m_F/m_B)^3$ in this limit.

In the opposite limit of large m_B/m_F, the ratio m_F/m_r slowly increases and eventually saturates to 1 for large m_B,

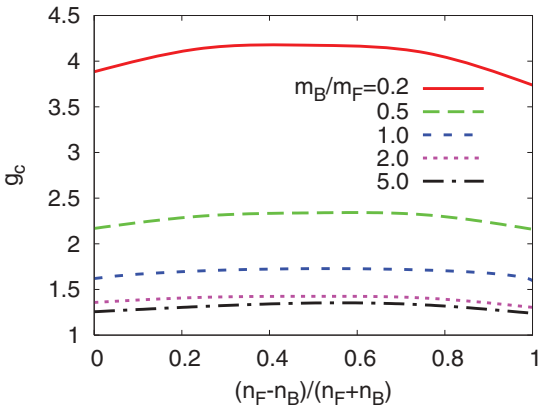

FIG. 5. (Color online) Critical coupling g_c as a function of density imbalance $(n_F - n_B)/(n_F + n_B)$ for different values of mass ratio m_B/m_F.

such that $|\mu_B|/E_F$ follows the slow logarithmic increase of g_c in this limit.

The fermionic chemical potential (reported in the inset) depends weakly on the mass imbalance, reflecting the weak dependence on g_c. As a matter of fact, the fermion chemical potential is determined essentially by the fermion density n_F, independently from the coupling value or mass ratio.

B. Momentum distribution functions

We pass now to study the momentum distribution functions $n_B(|\mathbf{q}|)$ and $n_F(|\mathbf{k}|)$ for bosons and fermions, as obtained from Eqs. (13) and (14), respectively. We present results for a density imbalance $(n_F - n_B)/(n_F + n_B) = 0.75$ to emphasize an interesting behavior of the bosonic momentum distribution function, which occurs only for a sufficiently large imbalance.

One can see, indeed, from Fig. 7 that the bosonic momentum distribution function vanishes identically at low momenta. This empty region extends from $|\mathbf{q}| = 0$ up to a certain value $|\mathbf{q}| = q_0$, which is determined essentially only by the density imbalance (for the specific case of Fig. 7, $q_0 \simeq 0.55$).

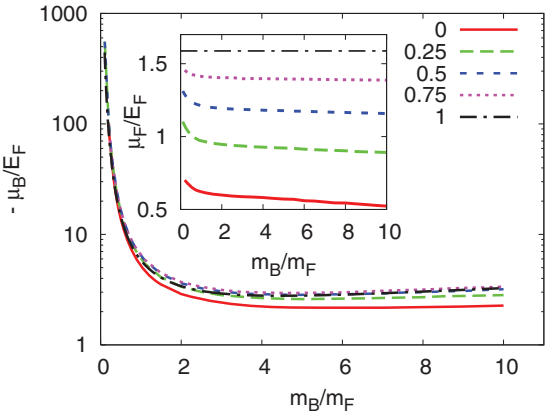

FIG. 6. (Color online) bosonic chemical potential at the critical coupling g_c as a function of mass ratio m_B/m_F for different values of density imbalance $(n_F - n_B)/(n_F + n_B)$. The corresponding fermionic chemical potential is reported in the inset.

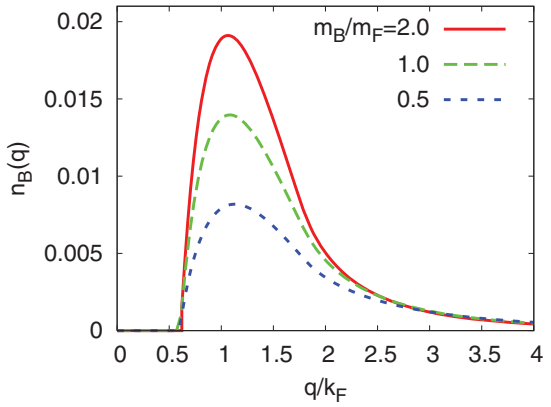

FIG. 7. (Color online) bosonic momentum distribution curves at g_c for a fixed density imbalance $(n_F - n_B)/(n_F + n_B) = 0.75$ and different values of the mass ratio (m_B/m_F).

The presence of the empty region can be interpreted as follows: For $n_F \gg n_B$, most fermions remain unpaired and fill a Fermi sphere of radius $k_{UF} \simeq [(n_F - n_B)/6\pi^2]^{1/3}$, as Fig. 8 for the fermionic distribution clearly shows. At g_c and larger couplings, the bosons are instead bound into molecules that, being composite fermions, fill a Fermi sphere with a radius $P_{CF} \simeq (n_B/6\pi^2)^{1/3}$. Now, as the region $|\mathbf{k}| < k_{UF}$ is already occupied by the unpaired fermions, only fermions with $|\mathbf{k}| > k_{UF}$ participate in the molecule. Since the momentum of the molecule is given by the sum $\mathbf{P} = \mathbf{q} + \mathbf{k}$, the constraints $|\mathbf{P}| < P_{CF}$ and $|\mathbf{k}| > k_{UF}$ then imply that only bosons with $|\mathbf{q}| > q_0 = k_{UF} - P_{CF}$ participate in the molecule, thus leaving empty the region $|\mathbf{q}| < q_0$.

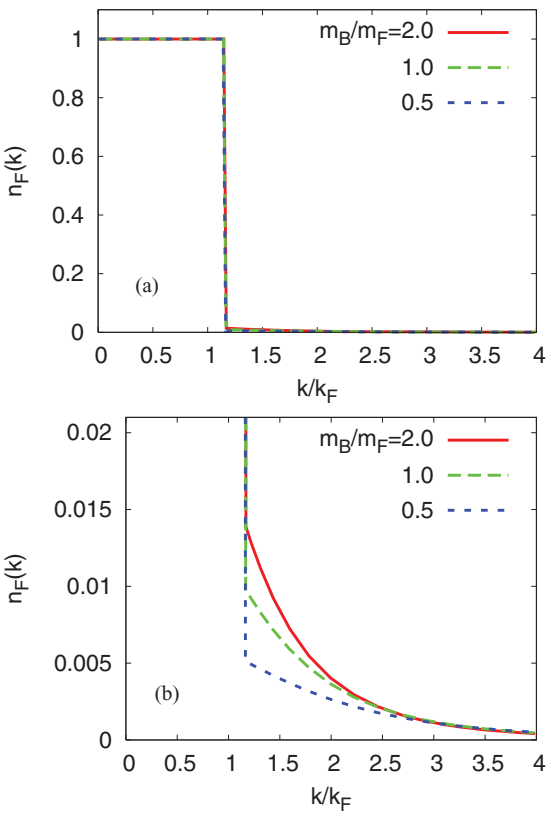

FIG. 8. (Color online) fermionic momentum distribution curves at g_c for a fixed density imbalance $(n_F - n_B)/(n_F + n_B) = 0.75$ and different values of the mass ratio m_B/m_F. The two panels correspond to a different choice of vertical scale.

We have verified that the equation $q_0 = k_{UF} - P_{CF}$ reproduces rather accurately the values of q_0 obtained numerically. In particular, the empty region does not exist at small density imbalance, when $k_{UF} < P_{CF}$. Note also that the initial rise of $n_B(|\mathbf{q}|)$ after the threshold q_0 is due to the progressive increase of the phase-space volume corresponding to the $\mathbf{q}$s satisfying the above constraints at a given $\mathbf{k}$. The saturation volume in phase-space is reached for $|\mathbf{q}|$ of the order of k_{UF}, after which $n_B(|\mathbf{q}|)$ starts to decrease, following eventually at sufficiently large wave vectors a molecular-like internal wave function $n_B(|\mathbf{q}|) \simeq n_M|\phi(|\mathbf{q}|)|^2$, where $|\phi(|\mathbf{q}|)|^2$ can be approximated by the two-body normalized wave function $\phi(|\mathbf{q}|) = (8\pi a^3)^{1/2}/(\mathbf{q}^2a^2 + 1)$, while the coefficient $n_M \simeq n_B$ can be interpreted as the molecular density.

The above approximate expression for $n_B(|\mathbf{q}|)$ accounts for the main difference in the curves calculated at different mass ratios (namely, the decreasing height of the curves when the mass ratio is lowered) due to the strong dependence of g_c, and then of a, on the mass ratio. Note further that the same kind of behavior is seen in the fermionic distribution function at momenta $|\mathbf{k}| > k_{UF}$, as can be made evident from Fig. 8(b). The comparison between Figs. 8(b) and 7 shows indeed that the bosonic and fermionic distribution functions become identical as the momentum increases; at large momenta $n_F(|\mathbf{k}|) \sim n_B(|\mathbf{k}|) \sim C/\mathbf{k}^4$, consistent with the universal large momenta behavior established in Ref. [52]. In particular, within our approximation, one can prove by taking the large-$|\mathbf{k}|$ limit in our expressions that the "contact" constant C is given by $C = -4m_r^2 \int \frac{d^4P}{(2\pi)^4}\Gamma(P)e^{i\Omega 0^+}$. In the strong-coupling limit, where all bosons are bound into molecules, a comparison with the expression for the molecular internal wave function then leads to the equation $C = 8\pi n_B/a$. Figure 9 reports the contact constant C at g_c normalized to its strong-coupling limit value $8\pi n_B/a$, as a function of the mass ratio m_B/m_F for different values of the density imbalance. One can see that the constant C at g_c is close to its strong-coupling-limit expression for all cases considered, with the largest deviations occurring at

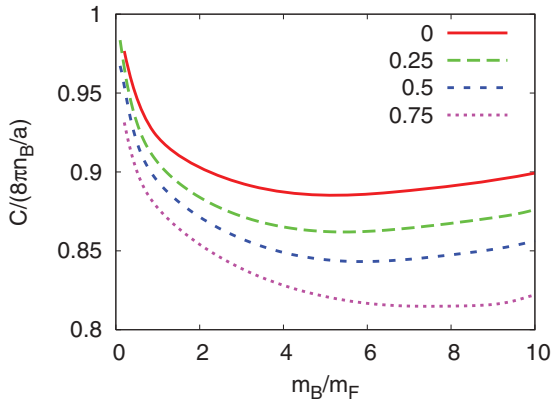

FIG. 9. (Color online) Contact constant C, normalized to its strong-coupling limit $8\pi n_B/a$, at g_c vs the mass ratio m_B/m_F for different values of density imbalance $(n_F - n_B)/(n_F + n_B)$.

intermediate values of mass ratio, as expected, since this is the region where g_c reaches its minimum and consequently the strong-coupling condition is less respected.

V. CONCLUDING REMARKS

In this paper, we studied a resonant Bose-Fermi mixture in the presence of a mass and/or density imbalance. We first analyzed the finite temperature phase diagram for the specific case of a ^{87}Rb-^{40}K mixture. We found that the overall shape of the phase diagram is similar to what was found previously for equal masses. The critical temperature starts from the noninteracting value ($T_0 = 3.31 n_B^{2/3}/m_B$) in the weak-coupling limit and eventually vanishes at a critical coupling g_c, when the effect of the boson-fermion coupling is so strong that the Bose-Einstein condensate is completely depleted. The critical temperature presents a weak maximum at intermediate coupling, not found for equal masses. We explained this feature as resulting from the balance between the hardening of the boson dispersion due to the boson-fermion interaction, and the condensate depletion due to molecular correlation. The predominance of one effect over the other depends on a fine tuning of the physical parameters, thus explaining the different behavior found for different cases.

We then considered the zero-temperature limit. We found that the critical coupling g_c is significantly affected by the mass imbalance, in particular for $m_B/m_F < 1$. In this case, for all values of the density imbalance, we obtained a rapid increase of g_c as $m_B/m_F \to 0$. We also found that the density imbalance influences only weakly the critical coupling, as previously found for equal masses [31]. On the other hand, a sufficiently large density imbalance produces quite a remarkable effect on the bosonic momentum distribution function. We found indeed that this function is completely depleted for momenta with magnitude below a certain value q_0. This value is set by the difference between the Fermi momenta associated with the unpaired fermions and the composite-fermions, respectively. Such a momentum distribution function reflects the constraints on the internal molecular wave function imposed by the presence of a large Fermi surface associated with the unpaired fermions. In this respect, the physics underlying this phenomenon is similar to that of the "Sarma phase" for a highly polarized Fermi gas in the strong-coupling limit of the BCS-BEC crossover [53–58]. In particular, the bosonic momentum distribution function is similar to the momentum distribution function of the minority species in a polarized Fermi gas. Interestingly, the fact that, in the present case, the molecules cannot condense, but rather fill a Fermi sphere, smears some features of the momentum distribution function but still preserves the presence of an empty region in the momentum distribution function. Such an interesting effect could be measured in a Bose-Fermi mixture in the molecular limit by using the same technique used to measure the momentum distribution of an ultracold Fermi gas in the BCS-BEC crossover [59].

ACKNOWLEDGMENTS

Partial support by the Italian MUR under Contract Cofin-2009 "Gas quantistici fuori equilibrio" is acknowledged.

APPENDIX: ONE-BOSON LIMIT

In this Appendix we consider the "one-boson" limit $(n_F - n_B)/(n_F + n_B) \to 1$ of our equations. In this limit the fermions become free due to the vanishing boson density. One has then $\Sigma_F = 0$ and $\mu_F = (6\pi^2 n_F)^{2/3}/(2m_F) = 2^{2/3} E_F$. The boson self-energy Σ_B remains instead finite and is determined by Eq. (11), with no simplifications with respect to the case at finite boson density. The full knowledge of Σ_B is, however, not necessary to calculate μ_B in the limit $n_B \to 0$. A study of the analytic structure of Σ_B in the complex frequency space along the lines of Ref. [43] shows that the limit $n_B \to 0$ corresponds, for $g > g_c$, to the requirement that the minimum of the composite fermion dispersion $\Omega_0(\mathbf{P})$ occurs exactly at zero frequency. By introducing the retarded composite-fermion propagator via the replacement $\Gamma^R(\mathbf{P},\omega) \equiv \Gamma(\mathbf{P}, i\Omega \to \omega + i0^+)$, the dispersion $\Omega_0(\mathbf{P})$ is determined by the pole of $\Gamma^R(\mathbf{P},\omega)$ in the complex plane. By assuming the minimum of $\Omega_0(|\mathbf{P}|)$ to occur at $\mathbf{P} = 0$, one has then the equation $\Gamma^R(0,0)^{-1} = 0$, which determines μ_B at a given coupling and mass ratio. The critical coupling g_c, on the other hand, is determined by the equation $\mu_B = \Sigma_B(0,0)$, as for finite density. In the limit $n_B \to 0$ only the pole of the fermionic Green's function contributes to the frequency integral in Eq. (11), yielding

$$\Sigma_B(0,0) = -\int \frac{d\mathbf{P}}{(2\pi)^3} \Theta\left[-\xi_F(\mathbf{P})\right] \Gamma^R\left(\mathbf{P}, \xi_F(\mathbf{P})\right), \quad \text{(A1)}$$

where

$$\Gamma^R(\mathbf{P},\xi_F(\mathbf{P})) = \left[-\frac{m_r}{2\pi a} \frac{m_r^{3/2}}{\sqrt{2}\pi} \sqrt{|\mu_B| - \frac{m_B \mathbf{P}^2}{2m_F M}} + I_F(\mathbf{P}) \right]^{-1}, \quad \text{(A2)}$$

and

$$I_F(\mathbf{P}) \equiv \int \frac{d\mathbf{p}}{(2\pi)^3} \frac{\Theta\left[-\xi_F\left(\frac{m_F}{M}\mathbf{P} - \mathbf{p}\right)\right]}{\frac{\mathbf{p}^2}{2m_r} - \frac{m_B}{m_F}\frac{\mathbf{P}^2}{2M} + |\mu_B|}. \quad \text{(A3)}$$

A calculation of the above integral yields

$$I_F(\mathbf{P}) = \frac{m_r k_{\mu_F}}{2\pi^2} + \frac{m_B L_{\mathbf{P}}}{4\pi^2} \frac{k_{\mu_F}^2 + 2m_r|\mu_B| - 2\left(\frac{\bar{m}}{M}|\mathbf{P}|\right)^2}{2|\mathbf{P}|} - \frac{m_r R_{\mathbf{P}}}{2\pi^2} \left[\arctan\left(\frac{k_{\mu_F} + \frac{m_F}{M}|\mathbf{P}|}{R_{\mathbf{P}}} \right) + \arctan\left(\frac{k_{\mu_F} - \frac{m_F}{M}|\mathbf{P}|}{R_{\mathbf{P}}} \right) \right], \quad \text{(A4)}$$

where $R_{\mathbf{P}} \equiv [2m_r|\mu_B| - (|\mathbf{P}|m_B/M)^2]^{1/2}$, while

$$L_{\mathbf{P}} \equiv \ln\left[\frac{\left(k_{\mu_F} + |\mathbf{P}|\right)\left(k_{\mu_F} + \frac{\delta m}{M}|\mathbf{P}|\right) + 2m_r|\mu_B|}{\left(k_{\mu_F} - |\mathbf{P}|\right)\left(k_{\mu_F} - \frac{\delta m}{M}|\mathbf{P}|\right) + 2m_r|\mu_B|} \right], \quad \text{(A5)}$$

where $\delta m = m_F - m_B$ and $\bar{m}^2 = (m_F^2 + m_B^2)/2$. By using the expressions (A2) to (A5), the self-energy $\Sigma_B(0,0)$ can then be calculated easily by a simple one-dimensional integral over $|\mathbf{P}|$. At g_c the equation $\mu_B = \Sigma_B(0,0)$ then yields

$$\mu_B = -\int_0^{k_{\mu_F}} \frac{d|\mathbf{P}|}{2\pi^2} \Gamma^R\left(|\mathbf{P}|, \xi_F(|\mathbf{P}|)\right). \quad \text{(A6)}$$

The equation $0 = \Gamma^{\mathrm{R}}(0,0)^{-1}$ yields finally

$$0 = -\frac{m_r}{2\pi a} + \frac{m_r^{3/2}}{\pi}\sqrt{|\mu|} + \frac{m_r}{\pi^2}\left[k_{\mu_{\mathrm{F}}} - 2\sqrt{m_r|\mu|}\arctan\left(\frac{k_{\mu_{\mathrm{F}}}}{2\sqrt{m_r|\mu|}}\right)\right]. \quad \text{(A7)}$$

The simultaneous solution of Eqs. (A6) and (A7) allows us to obtain g_c and μ_{B} for a given mass ratio. Note finally that, even though we have derived Eqs. (A6) and (A7) as a limiting case of our equations for a Bose-Fermi mixture, they describe also the polaron-to-molecule transition in a Fermi-Fermi mixture, since in this limit the statistics of the minority species becomes immaterial. We have verified, indeed, that our results for g_c in this limit agree with the results reported in Ref. [43] for the "first-level approximation."

1. Asymptotic expressions for g_c at small and large mass ratios

We conclude this Appendix by presenting the derivation of the asymptotic expressions (18) and (20). We assume μ_{B} to be large and negative as it occurs when g is large. The validity of this assumption is verified by the asymptotic expressions for g_c that are obtained accordingly. The chemical potential $\mu = (\mu_{\mathrm{B}} + \mu_{\mathrm{F}})/2$ is then also large and negative. By expanding Eq. (A7) in powers of $k_{\mu_{\mathrm{F}}}/\sqrt{m_r|\mu|}$ one obtains

$$2\mu \approx -\epsilon_0 + \frac{2}{3\pi m_r}k_{\mu_{\mathrm{F}}}^3 a, \quad \text{(A8)}$$

or, equivalently,

$$\mu_{\mathrm{B}} \approx -\epsilon_0 - \mu_{\mathrm{F}} + \frac{2}{3\pi m_r}k_{\mu_{\mathrm{F}}}^3 a. \quad \text{(A9)}$$

Note that the subleading term $\frac{2}{3\pi m_r}k_{\mu_{\mathrm{F}}}^3 a$ in Eq. (A8) describes the mean-field repulsion between the molecule forming in the strong-coupling limit and the fermions, as can be seen by casting it in the form $n_{\mathrm{F}}\frac{2\pi}{m_{\mathrm{MF}}}a_{\mathrm{MF}}$, where $m_{\mathrm{MF}} = Mm_{\mathrm{F}}/(m_{\mathrm{F}} + M)$ is the reduced mass of a molecule and one fermion, while

$$a_{\mathrm{MF}} = \frac{(1 + m_{\mathrm{F}}/m_{\mathrm{B}})^2}{1/2 + m_{\mathrm{F}}/m_{\mathrm{B}}}a \quad \text{(A10)}$$

is the molecule-fermion scattering length within the Born approximation [60].

The large negative value of μ_{B} then implies $I_{\mathrm{F}}(\mathbf{P}) \approx n_{\mathrm{F}}/|\mu_{\mathrm{B}}| \approx n_{\mathrm{F}}/\epsilon_0$, as can be seen more easily directly from Eq. (A3). The expansion of (A2) for $|\mu_{\mathrm{B}}|$ large then yields

$$\Gamma^{\mathrm{R}}(\mathbf{P}, \xi_{\mathrm{F}}(\mathbf{P})) \approx \frac{2\pi}{m_r^2 a}\frac{1}{\mu_{\mathrm{F}} - \alpha\mathbf{P}^2}, \quad \text{(A11)}$$

where we have used Eq. (A8), and $\alpha \equiv m_{\mathrm{B}}/(2Mm_{\mathrm{F}})$. By using Eq. (A1) we obtain

$$\Sigma_{\mathrm{B}}(0,0) \approx \frac{1}{\alpha\pi m_r^2 a}\left[k_{\mu_{\mathrm{F}}} + \frac{\sqrt{\mu_{\mathrm{F}}/\alpha}}{2}\ln\frac{\sqrt{\mu_{\mathrm{F}}/\alpha} - k_{\mu_{\mathrm{F}}}}{k_{\mu_{\mathrm{F}}} + \sqrt{\mu_{\mathrm{F}}/\alpha}}\right] = \frac{k_{\mu_{\mathrm{F}}}}{\alpha\pi m_r^2 a}\left[1 + \frac{\sqrt{1 + \frac{m_{\mathrm{F}}}{m_{\mathrm{B}}}}}{2}\ln\frac{\sqrt{1 + \frac{m_{\mathrm{F}}}{m_{\mathrm{B}}}} - 1}{\sqrt{1 + \frac{m_{\mathrm{F}}}{m_{\mathrm{B}}}} + 1}\right]. \quad \text{(A12)}$$

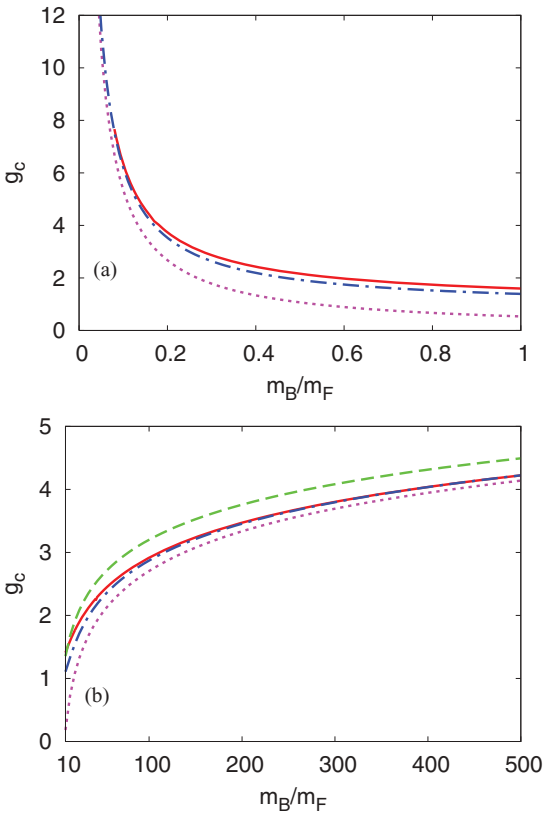

FIG. 10. (Color online) (a) Asymptotic expression (A15) for g_c at small mass ratios (dashed-dotted line) compared with full numerical solution (full line). The dotted curve is obtained by neglecting the subleading term within the brackets in (A15). (b) The asymptotic expression (A21) for g_c at large mass ratios (dashed-dotted line) is compared with the full numerical solution (full line). The dashed curve is obtained by neglecting the second and third terms on the right-hand side of (A21), while the dotted curve neglects only the third term.

By expanding the expression (A12) for a *small* mass ratio $m_{\mathrm{B}}/m_{\mathrm{F}} \ll 1$, we obtain

$$\Sigma_{\mathrm{B}}(0,0) \approx \frac{k_{\mu_{\mathrm{F}}}}{\alpha\pi m_r^2 a}\left[-\frac{1}{3}\frac{m_{\mathrm{B}}}{m_{\mathrm{F}}} + \frac{2}{15}\left(\frac{m_{\mathrm{B}}}{m_{\mathrm{F}}}\right)^2\right] \approx -\frac{2^{4/3}}{3\pi}\frac{k_{\mathrm{F}}}{am_{\mathrm{B}}}\frac{m_{\mathrm{F}}}{m_{\mathrm{B}}}\left(1 + \frac{8}{5}\frac{m_{\mathrm{B}}}{m_{\mathrm{F}}}\right). \quad \text{(A13)}$$

The equation $\mu_{\mathrm{B}} = \Sigma_{\mathrm{B}}(0,0)$ then yields

$$\epsilon_0 = \frac{2^{4/3}}{3\pi}\frac{k_{\mathrm{F}}}{am_r}\frac{m_{\mathrm{F}}}{m_{\mathrm{B}}}\left(1 + \frac{8}{5}\frac{m_{\mathrm{B}}}{m_{\mathrm{F}}}\right), \quad \text{(A14)}$$

where we have kept only the leading term in the expression (A9) for μ_{B} (the term μ_{F} would give a correction of order $(m_{\mathrm{B}}/m_{\mathrm{F}})^2$ to the asymptotic expression for g_c, with the last term in (A9) contributing an even smaller correction). By substituting $\epsilon_0 = 1/(2m_r a^2)$ we obtain then

$$\frac{1}{k_F a} = \frac{4 \times 2^{1/3}}{3\pi}\frac{m_{\mathrm{F}}}{m_{\mathrm{B}}}\left(1 + \frac{8}{5}\frac{m_{\mathrm{B}}}{m_{\mathrm{F}}}\right), \quad \text{(A15)}$$

which coincides with expression (18) reported in Sec. IV, and gives a large value of g_c for small mass ratios, consistently

with our starting assumption. The asymptotic expression (A15) is compared with the full numerical calculation of g_c in Fig. 10(a).

The expansion of Eq. (A12) for a *large* mass ratio $m_B/m_F \gg 1$ yields instead

$$\Sigma_B(0,0) \approx \frac{k_{\mu_F}}{\alpha\pi m_r^2 a}\left(1+\frac{1}{2}\ln\frac{m_F}{4m_B}\right) \tag{A16}$$

$$\approx \frac{2^{4/3}}{\pi}\frac{k_F}{am_F}\left(1+\frac{1}{2}\ln\frac{m_F}{4m_B}\right), \tag{A17}$$

where we have disregarded corrections to (A17) smaller at least by a factor m_F/m_B. By equating (A17) to (A9) we get then

$$\epsilon_0+\mu_F-\frac{2k_{\mu_F}^3 a}{3\pi m_r}=\frac{2^{\frac{4}{3}}}{\pi}\frac{k_F}{am_F}\left(-1+\frac{1}{2}\ln\frac{4m_B}{m_F}\right), \tag{A18}$$

yielding

$$\frac{1}{2a^2m_F}=\frac{2^{\frac{1}{3}}k_F}{\pi am_F}\left(\ln\frac{4m_B}{m_F}-2\right)-\frac{2^{\frac{2}{3}}k_F^2}{2m_F}+\frac{4k_F^3 a}{3\pi m_F}, \tag{A19}$$

from which, by multiplying both sides of Eq. (A19) by $2am_F/k_F$, we obtain

$$\frac{1}{k_Fa}=\frac{2^{\frac{4}{3}}}{\pi}\left(\ln\frac{4m_B}{m_F}-2\right)-2^{\frac{2}{3}}k_Fa+\frac{8\,(k_Fa)^2}{3\pi}, \tag{A20}$$

which shows that, to leading order, $g_c \approx (2^{4/3}/\pi)\ln(m_B/m_F)$ at large mass ratios. The slow ln dependence of g_c on m_B/m_F, however, makes it significant to keep also a few subleading corrections to the leading behavior. The solution of Eq. (A20) by iteration then yields

$$\frac{1}{k_Fa}=\frac{2^{\frac{4}{3}}}{\pi}\left(\ln\frac{4m_B}{m_F}-2\right)-\frac{2^{\frac{2}{3}}}{\frac{2^{\frac{4}{3}}}{\pi}\left(\ln\frac{4m_B}{m_F}-2\right)}+\frac{8}{3\pi}\frac{1}{\left[\frac{2^{\frac{4}{3}}}{\pi}\left(\ln\frac{4m_B}{m_F}-2\right)\right]^2}, \tag{A21}$$

which ignores corrections of order $1/(\ln\frac{m_B}{m_F})^3$ or higher and coincides with expression (20) reported in Sec. IV. The asymptotic expression (A21) is compared with the full numerical calculation of g_c in Fig. 10(b).

[1] L. Viverit, C. J. Pethick, and H. Smith, Phys. Rev. A **61**, 053605 (2000).
[2] X. X. Yi and C. P. Sun, Phys. Rev. A **64**, 043608 (2001).
[3] A. P. Albus, S. A. Gardiner, F. Illuminati, and M. Wilkens, Phys. Rev. A **65**, 053607 (2002).
[4] L. Viverit and S. Giorgini, Phys. Rev. A **66**, 063604 (2002).
[5] R. Roth and H. Feldmeier, Phys. Rev. A **65**, 021603(R) (2002).
[6] X.-J. Liu, M. Modugno, and H. Hu, Phys. Rev. A **68**, 053605 (2003).
[7] M. Lewenstein, L. Santos, M. A. Baranov, and H. Fehrmann, Phys. Rev. Lett. **92**, 050401 (2004).
[8] G. Modugno, G. Roati, F. Riboli, F. Ferlaino, R. J. Brecha, and M. Inguscio, Science **297**, 2240 (2002).
[9] D. B. M. Dickerscheid, D. van Oosten, E. J. Tillema, and H. T. C. Stoof, Phys. Rev. Lett. **94**, 230404 (2005).
[10] S. Powell, S. Sachdev, and H. P. Buchler, Phys. Rev. B **72**, 024534 (2005).
[11] A. V. Avdeenkov, D. C. E. Bortolotti, and J. L. Bohn, Phys. Rev. A **74**, 012709 (2006).
[12] D. C. E. Bortolotti, A. V. Avdeenkov, and J. L. Bohn, Phys. Rev. A **78**, 063612 (2008).
[13] F. M. Marchetti, C. J. M. Mathy, D. A. Huse, and M. M. Parish, Phys. Rev. B **78**, 134517 (2008).
[14] K. Günter, T. Stoferle, H. Moritz, M. Kohl, and T. Esslinger, Phys. Rev. Lett. **96**, 180402 (2006).
[15] C. Ospelkaus, S. Ospelkaus, L. Humbert, P. Ernst, K. Sengstock, and K. Bongs, Phys. Rev. Lett. **97**, 120402 (2006).
[16] S. Ospelkaus, C. Ospelkaus, L. Humbert, K. Sengstock, and K. Bongs, Phys. Rev. Lett. **97**, 120403 (2006).
[17] J. J. Zirbel, K.-K. Ni, S. Ospelkaus, J. P. D'Incao, C. E. Wieman, J. Ye, and D. S. Jin, Phys. Rev. Lett. **100**, 143201 (2008).
[18] K.-K. Ni, S. Ospelkaus, M. H. G. de Miranda, A. Pe'er, B. Neyenhuis, J. J. Zirbel, S. Kotochigova, P. S. Julienne, D. S. Jin, and J. Ye, Science **322**, 231 (2008).
[19] C.-H. Wu, I. Santiago, J. W. Park, P. Ahmadi, and M. W. Zwierlein, Phys. Rev. A **84**, 011601 (2011).
[20] J. W. Park, C.-H. Wu, I. Santiago, T. G. Tiecke, S. Will, P. Ahmadi, and M. W. Zwierlein, Phys. Rev. A **85**, 051602 (2012).
[21] M.-S. Heo, T. T. Wang, C. A. Christensen, T. M. Rvachov, D. A. Cotta, J.-H. Choi, Y.-R. Lee, and W. Ketterle, arXiv:1205.5304 (2012).
[22] S. Simonucci, P. Pieri, and G. C. Strinati, Europhys. Lett. **69**, 713 (2005).
[23] M. Y. Kagan, I. V. Brodsky, D. V. Efremov, and A. V. Klaptsov, Phys. Rev. A **70**, 023607 (2004).
[24] X. Barillier-Pertuisel, S. Pittel, L. Pollet, and P. Schuck, Phys. Rev. A **77**, 012115 (2008).
[25] L. Pollet, C. Kollath, U. Schollwöck, and M. Troyer, Phys. Rev. A **77**, 023608 (2008).
[26] M. Rizzi and A. Imambekov, Phys. Rev. A **77**, 023621 (2008).
[27] I. Titvinidze, M. Snoek, and W. Hofstetter, Phys. Rev. B **79**, 144506 (2009).
[28] F. M. Marchetti, T. Jolicoeur, and M. M. Parish, Phys. Rev. Lett. **103**, 105304 (2009).
[29] A. Storozhenko, P. Schuck, T. Suzuki, H. Yabu, and J. Dukelsky, Phys. Rev. A **71**, 063617 (2005).
[30] T. Watanabe, T. Suzuki, and P. Schuck, Phys. Rev. A **78**, 033601 (2008).
[31] E. Fratini and P. Pieri, Phys. Rev. A **81**, 051605(R) (2010).
[32] D. Ludwig, S. Floerchinger, S. Moroz, and C. Wetterich, Phys. Rev. A **84**, 033629 (2011).
[33] P. Pieri and G. C. Strinati, Phys. Rev. B **61**, 15370 (2000).

[34] Z.-Q. Yu, S. Zhang, and H. Zhai, Phys. Rev. A **83**, 041603(R) (2011).
[35] See, e.g., Chap. 6 of V. N. Popov, *Functional Integrals and Collective Excitations* (Cambridge University Press, Cambridge, 1987).
[36] See, e.g., Sec. 29 of A. Fetter and J. D. Walecka, *Quantum Theory of Many-Particle Systems* (Mc-Graw Hill, New York, 1971); J. M. Luttinger and J. C. Ward, Phys. Rev. **118**, 1417 (1960); Problems in the replacement of the frequency sums with integrals, in the zero-temperature limit, normally arise in the presence of double (or higher) poles of the summands in the complex frequency plane. We have not met these type of singularities in our case. In any case, the good matching of the finite-temperature results with those obtained at zero temperature verify *a posteriori* the validity of the procedure.
[37] M. Holzmann, J. N. Fuchs, G. Baym, J. P. Blaizot, and F. Laloë, C. R. Phys. **5**, 21 (2004).
[38] N. V. Prokof'ev and B. V. Svistunov, Phys. Rev. B **77**, 125101 (2008).
[39] M. Veillette, E. G. Moon, A. Lamacraft, L. Radzihovsky, S. Sachdev, and D. E. Sheehy, Phys. Rev. A **78**, 033614 (2008).
[40] P. Massignan, G. M. Bruun, and H. T. C. Stoof, Phys. Rev. A **78**, 031602(R) (2008).
[41] C. Mora and F. Chevy, Phys. Rev. A **80**, 033607 (2009).
[42] M. Punk, P. T. Dumitrescu, and W. Zwerger, Phys. Rev. A **80**, 053605 (2009).
[43] R. Combescot, S. Giraud, and X. Leyronas, Europhys. Lett. **88**, 60007 (2009).
[44] A. Schirotzek, C.-H. Wu, A. Sommer, and M. W. Zwierlein, Phys. Rev. Lett. **102**, 230402 (2009).
[45] C. J. M. Mathy, M. M. Parish, and D. A. Huse, Phys. Rev. Lett. **106**, 166404 (2011).
[46] J.-L. Song and F. Zhou, Phys. Rev. A **84**, 013601 (2011).
[47] E. Braaten and H. W. Hammer, Phys. Rep. **428**, 259 (2006).
[48] M. Correggi, G. Dell'Antonio, D. Finco, A. Michelangeli, and A. Teta, arXiv:1201.5740 (2012).
[49] O. I. Kartavtsev and A. V. Malykh, J. Phys. B **40**, 1429 (2007).
[50] M. M. Parish, Phys. Rev. A **83**, 051603 (2011).
[51] F. Chevy, Phys. Rev. A **74**, 063628 (2006).
[52] S. Tan, Ann. Phys. (NY) **323**, 2952 (2008); **323**, 2971 (2008).
[53] G. Sarma, J. Phys. Chem. Solids **24**, 1029 (1963).
[54] P. Pieri and G. C. Strinati, Phys. Rev. Lett. **96**, 150404 (2006).
[55] D. E. Sheehy and L. Radzihovsky, Ann. Phys. (NY) **322**, 1790 (2007).
[56] L. Radzihovsky and D. E. Sheehy, Rep. Prog. Phys. **73**, 076501 (2010).
[57] F. Chevy and C. Mora, Rep. Prog. Phys. **73**, 112401 (2010).
[58] P. Pieri, D. Neilson, and G. C. Strinati, Phys. Rev. B **75**, 113301 (2007); A. L. Subasi, P. Pieri, G. Senatore, and B. Tanatar, *ibid.* **81**, 075436 (2010).
[59] C. A. Regal, M. Greiner, S. Giorgini, M. Holland, and D. S. Jin, Phys. Rev. Lett. **95**, 250404 (2005).
[60] M. Iskin and C. A. R. Sa de Melo, Phys. Rev. A **76**, 013601 (2007).